Regularizing the divergent structure of light-front currents

Bernard L. G. Bakker
Department of Physics and Astrophysics, Vrije Universiteit, De Boelelaan 1081, NL-1081 HV Amsterdam, The Netherlands

Ho-Meoyng Choi
Department of Physics, North Carolina State University, Raleigh, North Carolina 27695-8202
and Physics Department, Carnegie Mellon University, Pittsburgh, Pennsylvania 15213

Chueng-Ryong Ji
Department of Physics, North Carolina State University, Raleigh, North Carolina 27695-8202
(Received 15 August 2000; revised manuscript received 7 December 2000; published 7 March 2001)

The divergences appearing in the (3+1)-dimensional fermion-loop calculations are often regulated by smearing the vertices in a covariant manner. Performing a parallel light-front calculation, we corroborate the similarity between the vertex-smearing technique and the Pauli-Villars regularization. In the light-front calculation of the electromagnetic meson current, we find that the persistent end-point singularity that appears in the case of point vertices is removed even if the smeared vertex is taken to the limit of the point vertex. Recapitulating the current conservation, we substantiate the finiteness of both valence and nonvalence contributions in all components of the current with the regularized bound-state vertex. However, we stress that each contribution, valence or nonvalence, depends on the reference frame even though the sum is always frame independent. The numerical taxonomy of each contribution including the instantaneous contribution and the zero-mode contribution is presented in the π, K, and D-meson form factors.

DOI: 10.1103/PhysRevD.63.074014 PACS number(s): 12.38.Lg, 11.10.−z, 11.30.Cp, 11.40.−q

I. INTRODUCTION

With the recent advances in the Hamiltonian renormalization program, light-front dynamics (LFD) appears to be a promising technique to impose the relativistic treatment of hadrons. In LFD a Fock-space expansion of bound states is made to handle the relativistic many-body effects in a consistent way [1]. The wave function $\psi_n(x_i,\vec{k}_{i\perp},\lambda_i)$ describes the component with n constituents, with longitudinal momentum fraction x_i, perpendicular momentum $\vec{k}_{i\perp}$ and helicity λ_i, $i=1,\ldots,n$. It is the aim of LFD to determine those wave functions and use them in conjunction with hard scattering amplitudes to describe the properties of hadrons and their response to electroweak probes. Important steps were taken towards a realization of this goal [2]. However, at present there are no realistic results available for wave functions of hadrons based on QCD alone. In order to calculate the response of hadrons to external probes, one might resort to the use of model wave functions. The variational principle enabled the solution of a QCD-motivated effective Hamiltonian and the constructed LF quark-model provided a good description of the available experimental data spanning various meson properties [3]. The same reasons that make LFD so attractive to solve bound-state problems in field theory make it also useful for a relativistic description of nuclear systems. Presently, it is realized that a parametrization of nuclear reactions in terms of non-relativistic wave functions must fail. LF methods have the advantage that they are formally similar to time-ordered many-body theories, yet provide relativistically invariant observables. Furthermore, as far as the concerned amplitude is unconditionally (or absolutely) convergent, the LF Hamiltonian approach must yield the same result as the one obtained by a covariant Feynman approach.

However, not all is well. As we have recently shown [4], the amplitudes that are only conditionally convergent must be treated with care. A case in point discussed in our work [4] was the calculation of a current matrix element in quantum field theory. A typical amplitude is given by the triangle diagram. One encounters this diagram e.g. when computing the meson form factor [see Fig. 1(a)]. The vertices denoted by Φ are coupling constants in covariant perturbation theory. The hard scattering process is the absorption of a photon of momentum q by a (anti-)quark. In the LFD approach the covariant amplitude is replaced by a series of LF time-ordered diagrams. In the case of the triangle diagram they are depicted in Figs. 1(b) and 1(c). The first [Fig. 1(b)] of these two diagrams is easily interpreted in terms of the LF wave functions Ψ. However, the other diagram [Fig. 1(c)] has one vertex that can again be written in the same way as before, but it contains also another vertex, denoted by Ψ', that cannot be written as a LF wave function. The necessity of this new element Ψ' in LFD has also been discussed in the cases of semileptonic meson decays [5] and deeply virtual Comp-

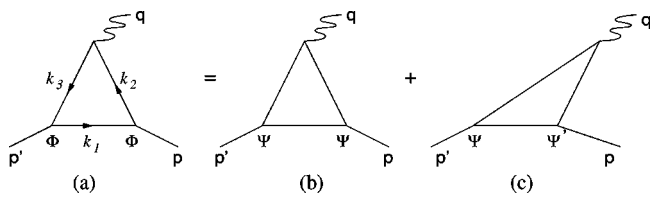

FIG. 1. Covariant triangle diagram (a) is equal to the sum of two light-front time-ordered diagrams, i.e., valence (b) and nonvalence (c) diagrams.

ton scattering [6]. One may call Ψ and Ψ' the vertices of leading order and non-leading order, respectively, in the sense that the leading order vertex corresponds to the lowest Fock state whereas the non-leading order vertex takes into account the higher Fock states. The diagrams with Ψ' are designated as *nonvalence* diagrams while those with vertices of type Ψ only are designated as *valence* diagrams. In order to obtain the invariant form factor, the two LF form factors must be added. It depends on the situation whether one can limit oneself to a single component of the current J^μ to extract the invariant objects. For the electromagnetic current of a spin-0 particle any single component would suffice to extract the unique form factor. On the other hand, in situations like semileptonic pseudoscalar meson decay, which involves two independent form factors, or the electromagnetic current of a (axial-)vector particle that is described by three independent form factors, one must use information from several current components to determine the invariant amplitudes.

Earlier, we presented an analysis of contributions from the nonvalence diagrams [4]. We constructed both leading and non-leading order vertices using pointlike covariant ones. The model that we used was essentially an extension of Mankiewicz and Sawicki's $(1+1)$-dimensional quantum field theory model [7], which was later reinvestigated by several others [8–12]. While their model [7] was a simple $(1+1)$-dimensional scalar field theory, it included a binding effect of the two-body bound state. Indeed, in Ref. [9], the relativistic two-body bound-state form factor was discussed in the full range of the binding energy. The starting model wave function was the solution of the covariant Bethe-Salpeter equation in the ladder approximation with a relativistic version of the contact interaction [9]. The covariant model wave function was a product of two free single particle propagators, the overall momentum-conserving Dirac delta function, and a constant vertex function. Consequently, all our form factor calculations were various ways of evaluating the Feynman triangle diagram in quantum field theory. As pointed out in Ref. [13], however, the elastic electromagnetic form factors of a bound-state computed from the triangle diagram and from the Hamiltonian front-form dynamics are the same [14]. Since our aim was to analyze the taxonomy of the triangle diagram, we didn't choose any particular gauge for the electromagnetic gauge field but presented the equivalence of the physical form factor $F(q^2)$ in any choice of the electromagnetic gauge[1] or in any choice of the current component.

Our conditionally convergent example of LFD with a fermion-loop showed that the bad component of the current, J^-, with spin-1/2 constituents exhibits a persistent end-point singularity in the contribution from the nonvalence diagram [4]. However, the calculation carried out so far was semi-realistic as the model was $(1+1)$-dimensional and only a point-vertex was considered.

In the present work, we extend our analysis of the fermion-loop to the case of $3+1$ dimensions. In $3+1$ dimensions both the covariant and the LF calculations are divergent and the model without any smeared vertex for the fermion loop is not well defined. In the recent literature [15,16], the fermion-loop was regulated by smearing the $q\bar{q}$ bound-state vertex in a covariant manner. However, the vertex function was not symmetric in the four momenta of the constituent quarks and could hardly be considered a realistic approximation of a $q\bar{q}$ bound state. It was regarded only as a convenient cutoff prescription which makes the one-loop integrals finite [15,16]. Furthermore, the calculation of the meson decay constant reveals that the end-point singularity is not completely canceled by such an asymmetric choice of the vertex function. (See the next section for more details.) We show in this work that the fermion-loop can also be regulated by taking a non-local gauge-boson vertex. With this method satisfying the Ward-Takahashi (WT) identity [17], we found the complete cancellation of the end-point singularity not only in the electromagnetic form factor but also in the decay constant. The non-local gauge-boson vertex remedies also the conceptual difficulty associated with the asymmetric way of treating q and $\bar{q}$ in the previous calculations [15,16].

Nevertheless, one should distinguish the bound state from the confined state. In this work, we are treating the mesons as bound states rather than confined states, because we do not yet know how to make a covariant regularization for the confined-state. Thus, our emphasis here is the inclusion of the non-leading order vertex rather than the model-building of a realistic meson wave function.

We have performed the LF calculation in parallel to the covariant Feynman calculation. Our light-front results entail the similarity between the vertex-smearing-technique (either for the bound-state vertex or the gauge-boson vertex) and the Pauli-Villars regularization. For the bosonic loop calculation, the two methods turn out to be identical. However, for the fermionic loop calculation, the vertex-smearing-technique shares only the same structure of the denominators with the Pauli-Villars regularization. Using the gauge-boson vertex-smearing technique, we found that the persistent end-point singularity is removed even if the smeared vertex is taken to the limit of the point vertex.

A significant entity of our work is the taxonomy of valence and nonvalence contributions substantiating the finiteness of each contribution when the gauge-boson vertex is regulated. Our results satisfy current conservation. However, we note that each contribution individually depends on the reference frame even though the sum is always frame independent. We thus elaborate the frame dependence of individual contributions. Also, the zero-mode contribution should be distinguished from the instantaneous contribution. For the numerical estimates of physical observables, we present the electromagnetic form factors of the π, K, and D mesons.

In the next section (Sec. II), we present both the covariant Feynman calculations and the LF calculations using the LF

[1]For a recent advocacy of the anti-light-cone gauge, $A^-=0$, see M. Morara, R. Soldati, and G. McCartor [in *New Directions in Quantum Chromodynamics*, edited by Chueng-Ryong Ji and Dong-Pil Min, AIP Conf. Proc. No. 494 (AIP, Melville, NY, 1999), pp. 284–290].

energy integration for the electromagnetic form factors of a pseudoscalar meson with spin-1/2 constituents. Section III contains the numerical taxonomy of both the valence and nonvalence diagrams to the electromagnetic form factors of π,K and D-mesons. The conclusion and discussion follow in Sec. IV. The general formula including unequal mass cases are summarized in Appendix A and the analytic behavior of the valence and nonvalence contributions at $Q^2 \to 0$ limit in various frames is summarized in Appendix B.

II. CALCULATIONS

The electromagnetic form factors can be extracted from the matrix elements of the current J^μ:

$$\langle p' | J^\mu | p \rangle = i e_m (p'^\mu + p^\mu) F(q^2), \tag{2.1}$$

where e_m is the charge of the meson and $q^2 = (p'-p)^2$ is the square of the four momentum transfer. If one uses the plus-component, $J^+ = J^0 + J^3$, the LF calculation gives two finite contributions, the *LF valence form factor* and the *LF nonvalence form factor*, that add up to the covariant result, as expected. The importance of the nonvalence contribution varies strongly with the momentum transfer and depends sensitively on the binding energy of the meson. For small values of q^2 and small binding energy, the valence part is dominant, but elsewhere the nonvalence diagram is essential for agreement between the LF calculation and the covariant results.

The form factor can also be extracted from the minus-component of the current, $J^- = J^0 - J^3$. Covariance guarantees that it makes no difference whether the form factor is determined using the plus or the minus current matrix element. As LFD is not manifestly covariant, it may happen that J^- leads to a form factor different from the one determined using J^+. As we showed in Ref. [4], the matrix element of J^- diverges even in (1+1)-dimensional LFD. Unless one regulates J^-, the current cannot be conserved. To assure current conservation, it was crucial to identify the term that causes the divergence. We have identified this term exactly and found that it is an infinite function of the momentum transfer. If this infinite term is subtracted, the two LF contributions become finite as it must be in a conserved current. Moreover, their sum equals again the covariant result as expected. Still, the regularized LF contributions obtained from J^- are different from the ones extracted from the plus current. The differences grow with increasing binding energy.

The covariant fermion triangle-loop [Fig. 1(a)] in 3+1 dimension is divergent if all the vertices are point-like. In the recent literature [15,16], the fermion-loop was regulated by smearing the $q\bar{q}$ bound-state vertex in a covariant manner. However, the vertex function used in Refs. [15,16] was not symmetric in the four momenta of the constituent quarks as we discussed in the Introduction. We note that the conceptual difficulty associated with the asymmetry could be remedied if the cutoff prescription is used in the gauge-boson vertex rather than in the $q\bar{q}$ bound-state vertex. In Fig. 1(a), we thus replace the point photon-vertex γ^μ by a non-local (or smeared) photon-vertex $S_\Lambda(k-p)\gamma^\mu S_\Lambda(k-p')$, where $S_\Lambda(p) = \Lambda^2/(p^2 - \Lambda^2 + i\epsilon)$ and Λ plays the role of a momentum cut-off. Our method is gauge invariant, and satisfies the WT identity [17]. Even though we have computed the covariant amplitude [Fig. 1(a)] with unequal constituent masses, for the clarity of presentation we will focus in this section on the equal mass case, i.e. $m_q = m_{\bar{q}} = m$. The basic formulas for the general case are given in the Appendix.

The covariant amplitude [Fig. 1(a)] for a pseudoscalar meson is given in the equal-mass case by

$$\langle p' | J^\mu | p \rangle = 4 N_c g^2 \Lambda^4 \int \frac{d^4k}{(2\pi)^4} \frac{(m^2 - k^2 + p\cdot p')k^\mu + (k^2 - m^2 - k\cdot p')p^\mu + (k^2 - m^2 - k\cdot p)p'^\mu}{D(k)D(k-p)D(k-p')D_\Lambda(k-p)D_\Lambda(k-p')}, \tag{2.2}$$

where N_c is the number of colors and g, modulo the obvious charge factor e_m is the normalization constant fixed by the unity of the form factor at zero momentum transfer and the denominator factor $D(k)$ from the quark propagator with momentum k is given by $D(k) = k^2 - m^2 + i\epsilon$. While the bound-state vertex is still pointlike, it satisfies a corresponding relativistic bound-state equation and a binding effect of the two-body bound state is thus included in our analysis. We note that one can split the denominators in Eq. (2.2) into four terms (see below) to show the similarity between the methods of photon-vertex-smearing and the Pauli-Villars regularization, namely the vertex-smearing-technique shares the same structure of the denominators with the Pauli-Villars regularization. To investigate the issue of the end-point singularity [4], we present the J^- calculation in the following.

First, the valence contribution shown in Fig. 1(b) is obtained in the range $0 < k^+ < p^+$. By picking up the pole of the spectator quark, i.e., $k^- = (m^2 + \vec{k}_\perp^2 - i\epsilon)/k^+$, we obtain

$$\langle p' | J^- | p \rangle = \frac{-4\pi i N_c g^2 \Lambda^4}{(\Lambda^2 - m^2)^2} \int \frac{dk^+ d^2\vec{k}_\perp}{(2\pi)^4} \frac{\{-k^+ p^- p'^- + \vec{k}_\perp \cdot \vec{p}'_\perp p^- + \vec{k}_\perp \cdot \vec{p}_\perp p'^- - \vec{p}_\perp \cdot \vec{p}'_\perp k^-\}}{k^+(k^+ - p^+)(k^+ - p'^+)}$$
$$\times \left[\frac{1}{E(p,\Lambda)E(p',\Lambda)} - \frac{1}{E(p,\Lambda)E(p',m)} - \frac{1}{E(p,m)E(p',\Lambda)} + \frac{1}{E(p,m)E(p',m)} \right], \tag{2.3}$$

where the energy denominator $E(p,\Lambda)$ is defined as

$$E(p,\Lambda)=\frac{m^2+\vec{k}_\perp^2}{k^+}-p^- -\frac{\Lambda^2+(\vec{k}_\perp-\vec{p}_\perp)^2}{k^+-p^+}. \tag{2.4}$$

As we see from Eq. (2.3), the result depends on the reference frame. However, as we will see later the sum of the valence and nonvalence contributions will of course be identical in any frame. In the present section, we choose the frame where $q^+=\alpha p^+$ and $\vec{p}_\perp=0$ and the momentum fraction x is defined by $k^+=(1-x)p^+$. Then the LF valence form factor [see Eq. (2.1)] is given by

$$\begin{aligned}F^-_{\rm val}(q^2)=&\frac{2N_c g^2\Lambda^4}{(2+\alpha)+\vec{q}_\perp^2/M^2}\int_0^1 dx\int\frac{d^2\vec{k}_\perp}{(2\pi)^3}\frac{(1-x)(M^2+\vec{q}_\perp^2)-(1+\alpha)\vec{k}_\perp\cdot\vec{q}_\perp}{(1-x)x^2(x+\alpha)^2}\\&\times\frac{1}{\left(\frac{m^2+\vec{k}_\perp^2}{1-x}+\frac{m^2+\vec{k}_\perp^2}{x}-M^2\right)\left(\frac{m^2+\vec{k}_\perp^2}{1-x}+\frac{\Lambda^2+\vec{k}_\perp^2}{x}-M^2\right)}\\&\times\frac{1}{\left(\frac{m^2+\vec{k}_\perp^2}{1-x}+\frac{m^2+(\vec{k}_\perp-\vec{q}_\perp)^2}{x+\alpha}-\frac{M^2+\vec{q}_\perp^2}{1+\alpha}\right)\left(\frac{m^2+\vec{k}_\perp^2}{1-x}+\frac{\Lambda^2+(\vec{k}_\perp-\vec{q}_\perp)^2}{x+\alpha}-\frac{M^2+\vec{q}_\perp{}^2}{1+\alpha}\right)},\end{aligned} \tag{2.5}$$

where M is the meson mass. The limit to the point vertex can be taken by letting $\Lambda\to\infty$ and we find that the result is finite in this frame.

Next, the nonvalence contribution shown in Fig. 1(c) is obtained in the range $p^+<k^+<p'^+$. Here, the pole is not taken as the spectator but as $k^-=p'^-+[m^2+(\vec{k}_\perp-\vec{p}'_\perp)^2-i\epsilon]/(k^+-p'^+)$ [for the term corresponding to the Pauli-Villars particle, $k^-=p'^-+[\Lambda^2+(\vec{k}_\perp-\vec{p}'_\perp)^2-i\epsilon]/(k^+-p'^+)$]. Following a procedure similar to the one described in the valence case, we find the LF nonvalence form factor to be given by

$$F^-_{\rm nv}(q^2)=-\frac{2N_c g^2\Lambda^4(1+\alpha)}{(\Lambda^2-m^2)[M^2(2+\alpha)+\vec{q}_\perp^2]}\int_0^\alpha dx\int\frac{d^2\vec{k}_\perp}{(2\pi)^3}\frac{1}{x^2(1+x)(\alpha-x)}\left[\frac{N(m)}{D0D1D2}-\frac{N(\Lambda)}{D5D3D4}\right], \tag{2.6}$$

where

$$N(m)=\left[m^2+\vec{k}_\perp^2-(1+x)\left(\frac{M^2+\vec{q}_\perp^2}{1+\alpha}-\frac{m^2+(\vec{k}_\perp-\vec{q}_\perp)^2}{\alpha-x}\right)\right]\left[\frac{m^2+(\vec{k}_\perp-\vec{q}_\perp)^2}{\alpha-x}+M^2\right]+\frac{(1+x)M^2(M^2+\vec{q}_\perp^2)}{1+\alpha}-\vec{k}_\perp\cdot\vec{q}_\perp M^2, \tag{2.7}$$

$$N(\Lambda)=\left[m^2+\vec{k}_\perp^2-(1+x)\left(\frac{M^2+\vec{q}_\perp^2}{1+\alpha}-\frac{\Lambda^2+(\vec{k}_\perp-\vec{q}_\perp)^2}{\alpha-x}\right)\right]\left[\frac{\Lambda^2+(\vec{k}_\perp-\vec{q}_\perp)^2}{\alpha-x}+M^2\right]+\frac{(1+x)M^2(M^2+\vec{q}_\perp{}^2)}{1+\alpha}-\vec{k}_\perp\cdot\vec{q}_\perp M^2,$$

$$D0=\frac{M^2+\vec{q}_\perp^2}{1+\alpha}-\frac{m^2+(\vec{k}_\perp-\vec{q}_\perp)^2}{\alpha-x}-\frac{m^2+\vec{k}_\perp^2}{1+x},$$

$$D1=M^2-\frac{M^2+\vec{q}_\perp^2}{1+\alpha}+\frac{m^2+(\vec{k}_\perp-\vec{q}_\perp)^2}{\alpha-x}+\frac{\Lambda^2+\vec{k}_\perp^2}{x},$$

$$D2=M^2-\frac{M^2+\vec{q}_\perp^2}{1+\alpha}+\frac{m^2+(\vec{k}_\perp-\vec{q}_\perp)^2}{\alpha-x}+\frac{m^2+\vec{k}_\perp^2}{x},$$

$$D5=\frac{M^2+\vec{q}_\perp^2}{1+\alpha}-\frac{\Lambda^2+(\vec{k}_\perp-\vec{q}_\perp)^2}{\alpha-x}-\frac{m^2+\vec{k}_\perp^2}{1+x},$$

$$D3=M^2-\frac{M^2+\vec{q}_\perp^2}{1+\alpha}+\frac{\Lambda^2+(\vec{k}_\perp-\vec{q}_\perp)^2}{\alpha-x}+\frac{\Lambda^2+\vec{k}_\perp^2}{x},$$

$$D4 = M^2 - \frac{M^2+\vec{q}_\perp^{\,2}}{1+\alpha} + \frac{\Lambda^2+(\vec{k}_\perp-\vec{q}_\perp)^2}{\alpha-x} + \frac{m^2+\vec{k}_\perp^{\,2}}{x}.$$

We find from Eq. (2.6) that the two terms in the integrand are individually finite as long as the parameter Λ is finite. There is neither an ultraviolet divergence nor an end-point singularity. However, in the limit to the point vertex (i.e. $\Lambda \to \infty$), we find that each term has not only a linear divergence in the $\vec{k}_\perp$ integration, but also an end-point singularity in the x integration, which cancel each other exactly. Thus, in the point vertex limit, we find that the end-point singularity is completely removed even though the result is logarithmically divergent as it must be in the (3+1)-dimensional fermion-loop with point vertices. This shows a striking difference from the calculation without relying on the vertex regularization from the beginning [4]. The critical reason for this is that the end-point singularity for the fermion-loop is a consequence of the bottomless nature of the Dirac sea and the vertex-smearing effectively provides the weighting in the Dirac sea deemphasizing the lower part. The previously identified end-point singularity [4] is exactly canceled by the identical end-point singularity from the term generated by the vertex-smearing corresponding to the Pauli-Villars particle. Therefore, in the regularized case, all the physical degrees of freedom are taken into account.

In addition, the sum of the valence and nonvalence contributions $F(q^2)=F_{\rm val}(q^2)+F_{\rm nv}(q^2)$ is of course identical to the results obtained by other components of the current, i.e. either J^+ or $J^\perp$ [15,16].[2] Also, the net result $F(q^2)$ is independent of the choice of reference frame.

A similar calculation can be made for the pseudoscalar-meson decay constant f. Taking a non-local gauge-boson vertex, we verified again the exact cancellation of linear and logarithmic divergences in the (two-point) fermion loop. The result for the equal mass case such as the pion is given by

$$f = \frac{N_c\, g\, m\Lambda^4}{4\sqrt{2}\pi^2(\Lambda^2-m^2)^2}\int_0^1 dx \log\left[\frac{C(m,m)C(\Lambda,\Lambda)}{C(m,\Lambda)C(\Lambda,m)}\right], \tag{2.8}$$

where $C(m_1,m_2)$ is given by

$$C(m_1,m_2) = x(1-x)M^2 - (1-x)m_1^2 - xm_2^2. \tag{2.9}$$

If the asymmetric $q\bar{q}$ bound-state vertex-smearing is used as in Refs. [15,16], the above result, Eq. (2.8), is replaced by

$$f = \frac{N_c\, g\, m\Lambda^2}{4\sqrt{2}\pi^2(\Lambda^2-m^2)}\int_0^1 dx \log\left[\frac{C(m,m)}{C(m,\Lambda)}\right]. \tag{2.10}$$

We note that the logarithmic divergence is not completely canceled in the unequal mass case if the minus component of the weak current is used with the asymmetric $q\bar{q}$ bound-state vertex smearing. The non-local gauge-boson vertex used in this work does not suffer from such an incomplete cancellation of divergences no matter which component of the current is used.

[2]In the electromagnetic form factor, there is no zero-mode contribution in the $J_\perp$ current.

TABLE I. Our model parameters of constituent quark masses m, and cutoff values Λ (in units of GeV) used in this work. The decay constants $f^{\rm sym}$ [$f^{\rm asym}$] obtained by Eq. (2.8) [Eq. (2.10)] are also compared with the experimental values $f^{\rm exp}$ [24].

Meson	m_q	Λ_q	$m_{\bar{q}}$	$\Lambda_{\bar{q}}$	$f^{\rm sym}[f^{\rm asym}]$	$f^{\rm exp}$[MeV]
π	0.25	0.90	0.25	0.90	92.5 [122.2]	92.4 ± 0.25
K	0.25	0.90	0.48	0.91	112.5 [139.4]	113.4 ± 1.1
D	1.78	1.79	0.25	0.90	108.6 [191.5]	$\leqslant 154.9$

In the next section, we present the numerical taxonomy of the π, K, and D meson electromagnetic LF form factors choosing various reference-frames, as well as the values of the decay constants f_π, f_K and f_D.

III. NUMERICAL RESULTS

In Table I, we present our model parameters such as the constituent quark masses (m), and the cutoff values (Λ), as well as the decay constants that we calculated here and compared to the experimental data [24]. The meson masses (M) are taken as the experimental values [24]. Our model parameters have been chosen to fit both the charge radii and the decay constants to the experimental data well, although the available data for the decay constant of the D-meson is only an upper limit. We also compare in Table I the decay constants from our symmetric non-local gauge-boson vertex ($f^{\rm sym}$) with those from the asymmetric $q\bar{q}$ bound-state vertex ($f^{\rm asym}$) smearing case. However, we note that our calculation here is limited in value because the zero-range approximation is used for the bound-state vertices.

Three different reference frames were considered: the Drell-Yan-West (DYW) frame, the target-rest frame (TRF) and the Breit frame. The corresponding kinematics is given in Table II. The DYW frame has gained some popularity in deep-inelastic scattering calculations because in that frame $q^+=0$ identically. This frame can be obtained by taking the

TABLE II. The kinematics in the reference frames used in this work, where $\kappa = Q^2/2M$ and $\hat{n}=(\cos\phi,\ \sin\phi)$.

Kinematics	Target rest frame	Breit frame	DYW frame
q^+	$\kappa + Q\sqrt{1+\kappa/2M}\cos\theta$	$+Q\cos\theta$	0
q^-	$\kappa - Q\sqrt{1+\kappa/2M}\cos\theta$	$-Q\cos\theta$	Q^2/p^+
$\vec{q}_\perp$	$Q\sqrt{1+\kappa/2M}\sin\theta\hat{n}$	$Q\sin\theta\hat{n}$	$Q\hat{n}$
p^+	M	$\sqrt{M^2+Q^2/4}-q^+/2$	p^+
p^-	M	$\sqrt{M^2+Q^2/4}-q^-/2$	M^2/p^+
$\vec{p}_\perp$	0	$-\vec{q}_\perp/2$	0

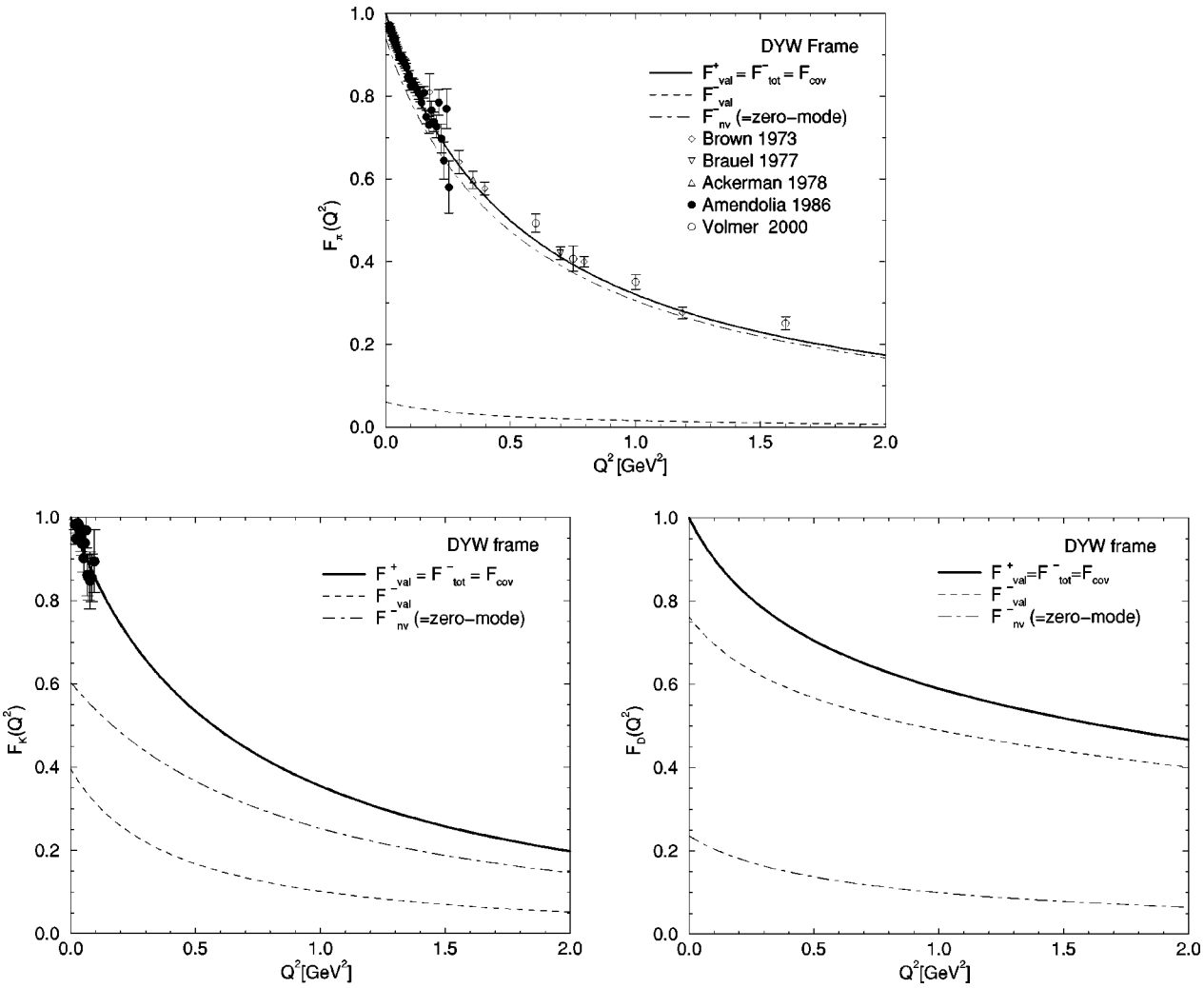

FIG. 2. Pion, *K*, and *D* meson form factors in the Drell-Yan-West (DYW) frame compared with experimental data for pion [18–22] and kaon [23]. The part $F^+_{\rm nv}$ vanishes identically in this reference frame.

$\alpha\to 0$ limit in the frame presented in Sec. II. In the limit $\alpha\to 1$, the frame presented in Sec. II coincides with the target-rest frame with $\theta=0$.

Now we comment on our results shown in the figures below. (In all of these figures, we use thick solid lines for the covariant form factor, thick dashed lines for $F^+_{\rm val}$, thick dot-dashed lines for $F^+_{\rm nv}$, thin dashed and dot-dashed lines for the corresponding minus LF form factors.) We show in Fig. 2 the results of our numerical calculations using the DYW frame and compare with the experimental data [18–23]. Our total results, represented by the solid line in each figure, are also in very good agreement with the experimental data of the pion and kaon form factors, respectively.

In the DYW frame $F^+_{\rm nv}$ vanishes identically. Remarkably, we find that the nonvalence part of the minus current, which in this reference frame coincides with the zero-mode contribution, makes a very important contribution to the total form factor and may even dominate over the valence part in the whole Q^2-range considered. There are quantitative differences between the results obtained for the different mesons, which are to a large extent due to the difference in binding: the tighter the binding, the more important $F^-_{\rm nv}$ becomes. We checked the binding effect in the case of the pion. By varying the quark mass alone from the realistic value of 0.25 GeV to 0.07007 GeV, thus lowering the binding energy to 0.1% of the pion mass, we found that the value of $F^-_{\rm val}$ at $Q^2=0$ was increased from 6% to 69%. Still, for $Q^2>0.3$ GeV^2 $F^-_{\rm val}$ is lower than $F^-_{\rm nv}$. This indicates that for the larger values of Q^2, the relativistic effects can still be large.

The frame dependence of the different components of the current can be studied by comparing the results of calculations in different frames and at different values of the polar angle θ. It is worth mentioning that the results must be independent of the azimuthal angle ϕ, because rotations about the *z*-axis are kinematical transformations. (We used this fact as a check on the correctness of our codes.)

In Fig. 3 we show the results of our numerical calculations in the Breit frame at $\theta=0$, which differs from the target-rest frame at $\theta=0$ by a boost in the *z*-direction only, so the results are identical in these two frames. The first

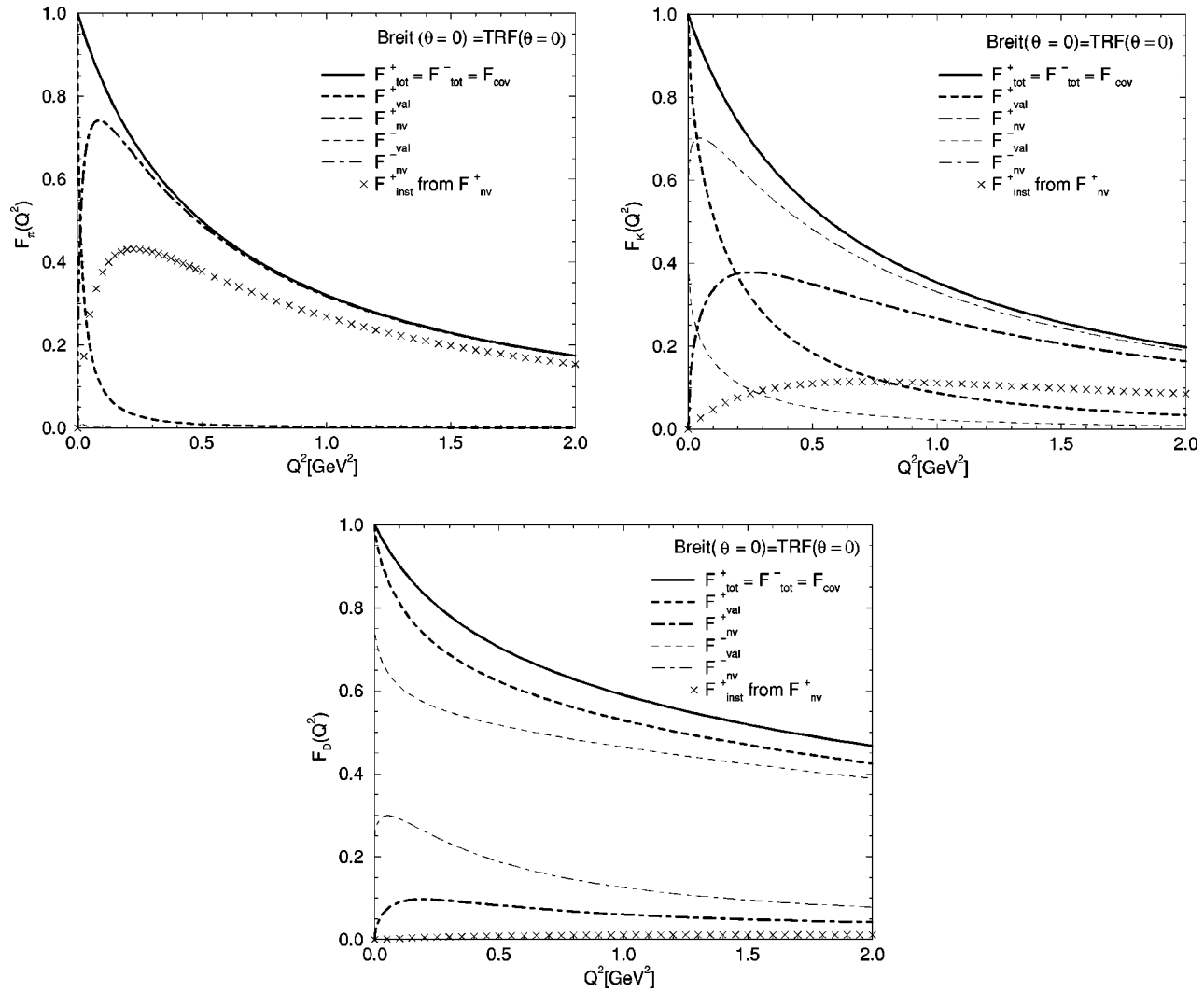

FIG. 3. Pion, *K*, and *D* meson form factors in the target-rest frame (TRF) or the Breit frame, both at $\theta=0$.

thing we notice is the great difference with the DYW frame. Now there is a sizable contribution from $F^+_{\rm nv}$, which dominates at higher values of the momentum transfer: at $Q^2=0$, $F^+_{\rm val}$ coincides with the covariant form factor. It crosses $F^+_{\rm nv}$ at some value of Q^2, the crossover point being smaller for larger binding energy. It is of special interest to separate the instantaneous part, i.e. the contribution to F^+ from diagrams with one internal instantaneous propagator. They are given in the figures by crosses ($\times$). It turns out that they give a very large contribution to the pion form factor but become negligible for the heavy *D*-meson case.

Turning to the minus current we see that in this reference frame the relative importance of $F^-_{\rm nv}$ becomes more prominent than in the DYW frame for the more tightly bound mesons π and *K*. In the case of the pion the dominance of $F^-_{\rm nv}$ is so strong that it can hardly be distinguished from the covariant form factor. The figures (in Fig. 3) suggest that at $Q^2=0$ the values obtained are frame independent. This is indeed the case as we found in our calculations and can be understood as the equality of the form factors in the long-wave-length limit.

A first glance at the angle dependence is given in Fig. 4. In both the target-rest frame and the Breit frame for $\theta=\pi/2$ the transferred momentum is purely transverse. As the pure Lorentz boosts in the transverse direction, K_1 and K_2, are dynamical in LFD, we must expect a strong frame dependence and this is indeed what we find. As $q^+=0$ in the Breit frame for $\theta=\pi/2$, the part $F^+_{\rm nv}$ vanishes identically. Still, the DYW frame results differ for the minus current, which is clear from a comparison with Fig. 2. The reason is that the minus component of the current in DYW frame is not proportional to the minus component of the current in the Breit frame for $\theta=\pi/2$. For the same reason the zero-mode contributions differ in the two frames. In the DYW frame it is very close to the total form factor, while in the Breit frame it even overshoots the covariant form factor at large values of Q^2 by a factor of almost 2. In this connection we want to mention the work of Frederico et al. [15], who performed a calculation similar in spirit to ours, but claimed that in the Breit frame at $\theta=\pi/2$ $F^-_{\rm val}$ is always very close to the covariant form factor. This discrepancy was due to the difference of their $F^-_{\rm val}$ definition in the Breit frame at $\theta=\pi/2$, where they removed the term that is odd under the transformation $p^- - k^- \rightarrow -(p^- - k^-)$ in their definition [25]. However, our

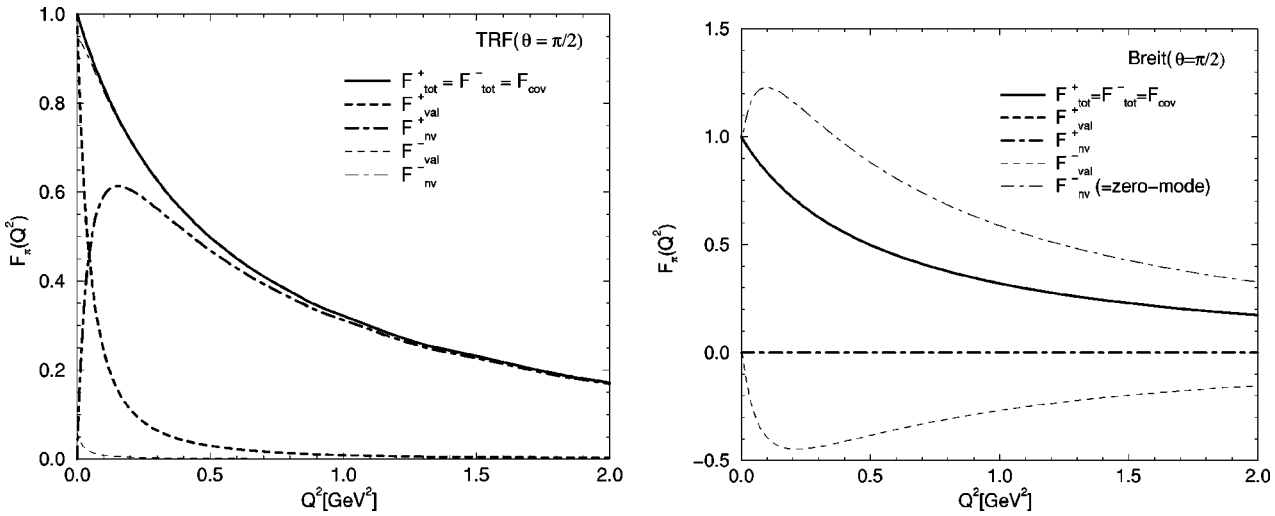

FIG. 4. Pion form factor in the target-rest frame and the Breit frame at $\theta=\pi/2$.

definition of $F^-_{\rm val}$ is general for any angle θ and our results on the θ-dependence are smooth as shown in Fig. 9.

We show the systematics of the angle dependence for the case of the pion only. Our results are depicted in Figs. 5–8. (The thick solid line for $\theta=0$, thin dotted line for $\theta=\pi/4$, the thick dashed line for $\theta=\pi/2$, the thin dot-dashed line for $\theta=3\pi/4$, and the thick long-dashed line for $\theta=\pi$.) One sees immediately that the angle dependence is smooth but can be very strong, both for the valence and the nonvalence parts, calculated from either the plus or the minus current.

One might try to exploit the angle dependence to optimize the calculation of the form factor in a noncovariant framework. However, as the figures above clearly show, there is no value for the angle θ where both $F^+_{\rm nv}$ and $F^-_{\rm nv}$ are negligible, or even suppressed, compared to the valence parts, for all values of Q^2. On the contrary, as the values of the form factor components at $Q^2=0$ are frame independent, we can be sure that $F^-_{\rm nv}$ must be very important for an important part of the Q^2 range.

As a summary of what we found concerning the angle dependence we show in Fig. 9 the complete angle dependence for two values of the momentum transfer, $Q^2=0$ and 0.1 GeV^2. All curves in this figure are clearly smooth and demonstrate the fact that there is no preferred value for the polar angle θ.

IV. CONCLUSION AND DISCUSSION

In this paper, we have analyzed all the components of the current quantized on the light-front to compute the electromagnetic form factors of pseudoscalar mesons with spin-1/2 constituents. Since our aim in this work was to analyze the taxonomy of the triangle diagram, we did not choose any particular electromagnetic gauge but just presented the equivalence of the physical form factor $F(q^2)$ in any choice of the current component. The divergence appearing in the (3+1)-dimensional fermion-loop calculations was regulated by the covariant vertex-smearing-technique. Performing the

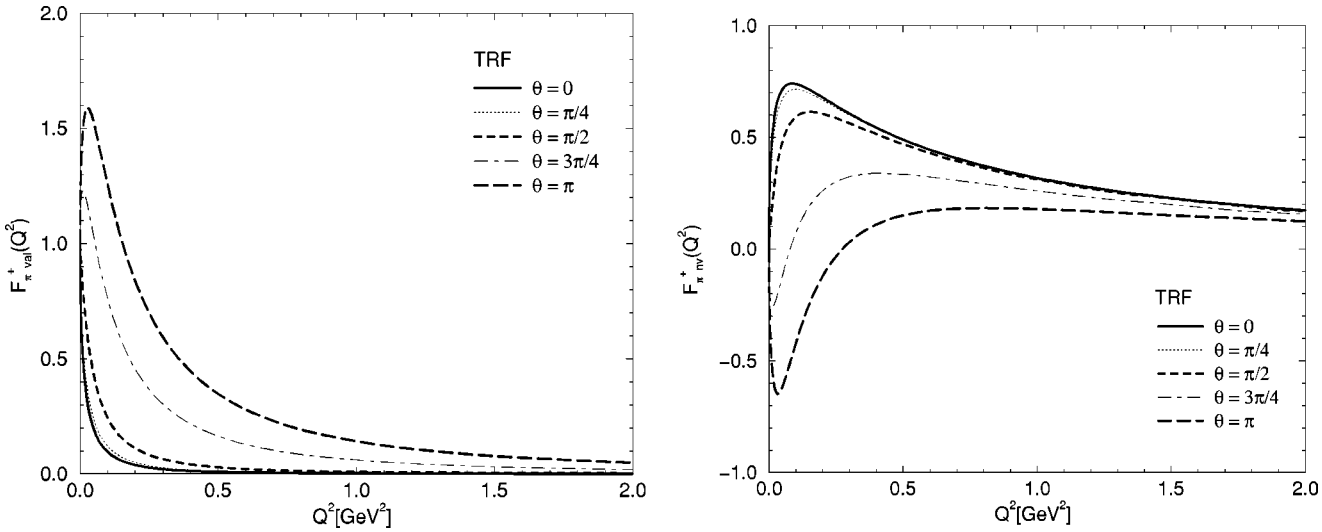

FIG. 5. Pion LF form factors $F^+_{\rm val}$ and $F^+_{\rm nv}$ in the target-rest frame for five different values of the polar angle θ.

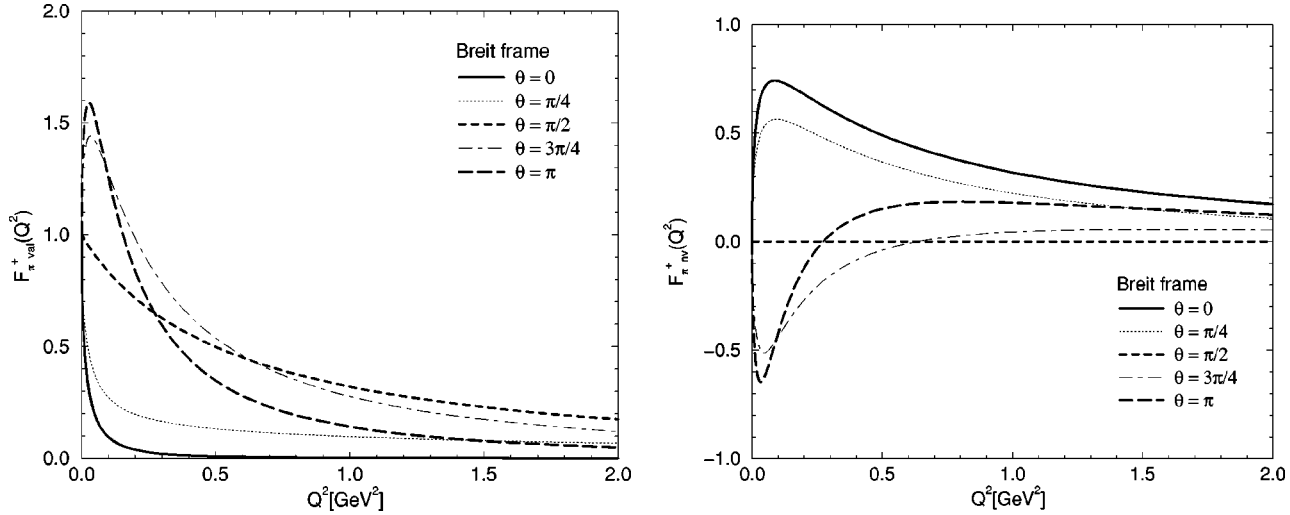

FIG. 6. Pion LF form factors $F^+_{\rm val}$ and $F^+_{\rm nv}$ in the Breit frame for five different values of the polar angle θ.

light-front calculation, we verified that the vertex-smearing-technique is similar to the Pauli-Villars regularization. In the J^- computation, we find that the critical smearing effect persists even in the limit to the point vertex because the end-point singularity existing otherwise is completely removed once the limit is taken at the end of the calculation. If the limit is taken at the beginning of the calculation, however, we have already shown that the end-point singularity in the nonvalence contribution leads to an infinitely different result from that obtained by the covariant Feynman calculation [4]. Our taxonomical analysis demonstrated that each individual contribution, whether valence or nonvalence, is finite regardless of which component of the current is considered. However, we stress that each contribution depends on the reference-frame even though the sum does not. Of course, the invariance of the sum ensures the current conservation. Also, the zero-mode contribution should be distinguished from the instantaneous contribution as we have numerically estimated the differences.

From our numerical calculations we can conclude that to obtain agreement with the covariant form factor one needs both the valence and the nonvalence parts. For tightly bound states the nonvalence parts dominate in an important part of the range of Q^2 values that we studied. It is natural that this result runs counter to nonrelativistic intuition, which says that the valence parts should dominate, because the tightly bound states are not expected to be non-relativistic. In Ref. [4] it was demonstrated in the $(1+1)$-dimensional case, that by weakening the binding $F^+_{\rm val}$ and $F^-_{\rm val}$ approximate the covariant form factor more and more closely. Here we found that indeed for less tightly bound states the valence parts come closer to the covariant result, but even at $Q^2=0$ $F^-_{\rm val}$ gives only 69% of the covariant form factor.

If two reference frames can be connected by a kinematical Lorentz transformation the LF form factors calculated in these two frames must be the same. Otherwise they must differ. We found that the angle dependence within a chosen reference frame is always smooth, although it may be very

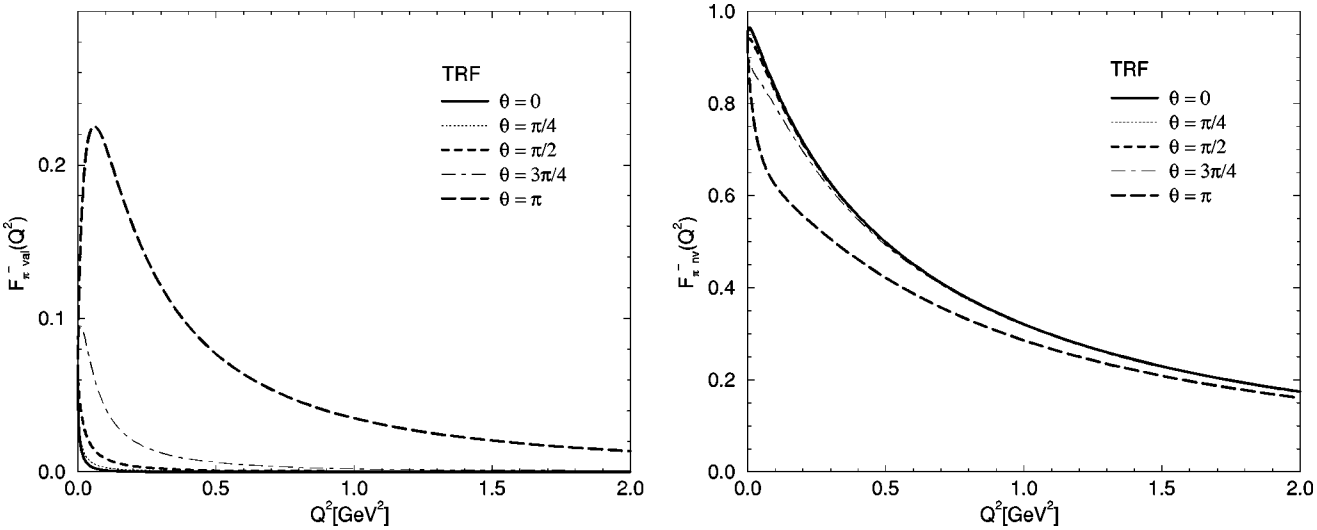

FIG. 7. Pion LF form factors $F^-_{\rm val}$ and $F^-_{\rm nv}$ in the target-rest frame for five different values of the polar angle θ.

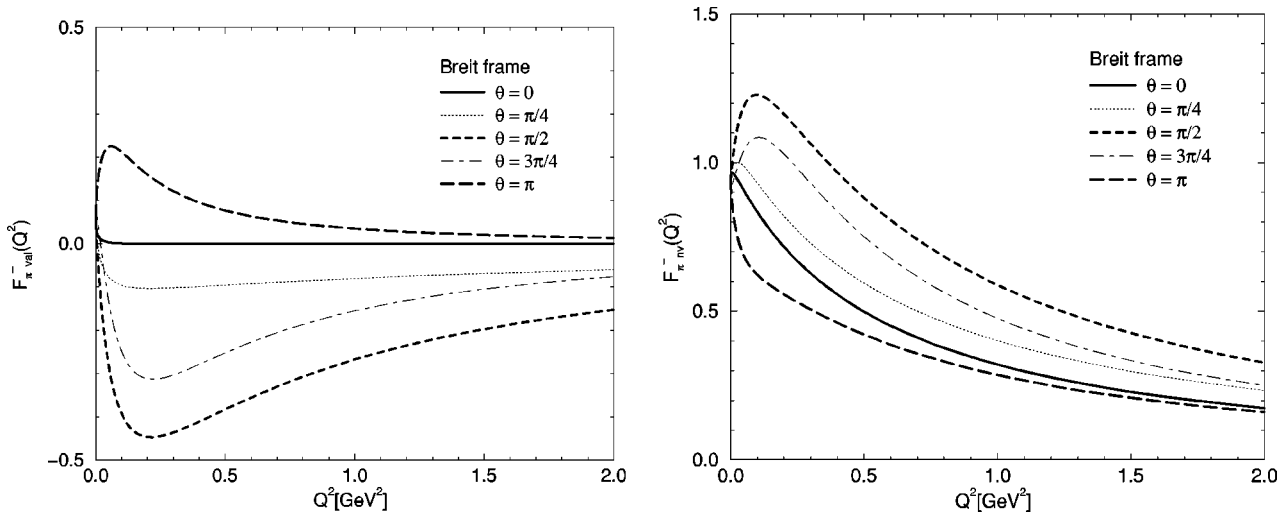

FIG. 8. Pion LF form factors $F^-_{\rm val}$ and $F^-_{\rm nv}$ in the Breit frame for five different values of the polar angle θ.

strong. For some values of the polar angle θ two reference frames may be connected by a kinematical Lorentz transformation, e.g., the target-rest frame and the Breit frame for $\theta=0$. On the other hand, the DYW frame and the Breit frame for $\theta=0$ are not connected by a kinematical transformation and the form factor components consequently do not coincide. More details of the frame-dependence can be found in Ref. [26].

While the calculations carried out in this work are more realistic than the $(1+1)$-dimensional case with the point vertex, they are still semi-realistic as the model uses a bound state rather than a confined state. Moreover, we used for the vertices those obtained from a Bethe-Salpeter equation using a contact interaction [7] which are of zero range and may emphasize the importance of the nonvalence contributions rather differently from a more realistic model. Thus, there is still much room for extending our model towards a more realistic model. However, the essential conclusions about the similarity to the Pauli-Villars regularization and the cancellations of both ultra-violet divergence and the end-point singularity remain intact. Nevertheless, the numerical results may differ from a more realistic model calculation. This point is presently under investigation.

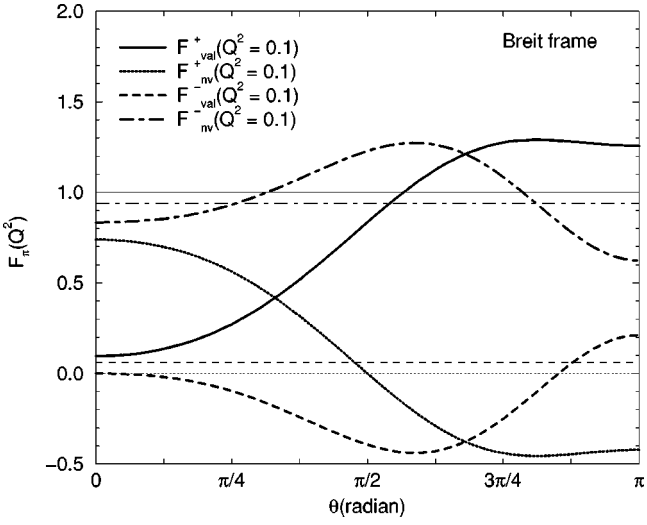

FIG. 9. Systematics of the angle dependence of the LF form factors at $Q^2=0.1$ GeV^2 (thick lines) and 0 GeV^2 (thin lines) in the Breit frame.

ACKNOWLEDGMENTS

This work was supported in part by a grant from the U.S. Department of Energy (DE-FG02-96ER 40947) and the National Science Foundation (INT-9906384). This work was started when H.M.C. and C.R.J. visited the Vrije Universiteit and they want to thank the staff of the Department of Physics at VU for their kind hospitality. B.L.G.B. wants to thank the staff of the Department of Physics at NCSU for their warm hospitality during a stay when this work was completed. The North Carolina Supercomputing Center and the National Energy Research Scientific Computer Center are also acknowledged for the grant of Cray time.

APPENDIX A: UNEQUAL-MASS CASE

If we number the momenta of the internal lines of the fermion triangle as k_1 (spectator), $k_2=p+k_1$, and $k_3=p'+k_1$ (struck quark) respectively, and the corresponding masses as m_1, m_2, and m_3, then we find for the trace appearing in the numerator of the covariant integral the expression

$$T^\mu=4[-(m_2m_3-k_2\cdot k_3)k_1^\mu+(m_1m_3-k_1\cdot k_3)k_2^\mu +(m_1m_2-k_1\cdot k_2)k_3^\mu]. \tag{A1}$$

The valence diagram is obtained if one calculates the integral over k_1^- by closing the contour around the pole corresponding to putting the spectator k_1 on the mass-shell. This corresponds to the following values for the minus components of the momenta to be used in the expression for T^μ:

$$k_1^- = \frac{\vec{k}_{1\perp}^2 + m_1^2}{k_1^+}, \quad k_2^- = p^- + k_1^-, \quad k_3^- = p'^- + k_1^-. \tag{A2}$$

To obtain the nonvalence diagram one closes the contour around the pole corresponding to k_3. Then one gets for the part of the propagator with the mass m_3

$$k_3^- = \frac{\vec{k}_{3\perp}^2 + m_3^2}{k_3^+}, \quad k_1^- = -p'^- + k_3^-, \quad k_2^- = p^- - p'^- + k_3^-. \tag{A3}$$

For the part of the propagator with the cutoff Λ' the same formula can be used, but with m_3 replaced by Λ'.

As the smearing we use affects only the denominator parts of the propagator of the struck quark, the replacement of m_3 by Λ' in T^μ occurs only in the minus components.

The energy denominators are easy to find. One obtains, for the valence parts,

$$D(k-p) = p^- + \frac{\vec{k}_{1\perp}^2 + m_1^2}{k_1^+} - \frac{\vec{k}_{2\perp}^2 + m_2^2}{k_2^+},$$

$$D(k-p') = p'^- + \frac{\vec{k}_{1\perp}^2 + m_1^2}{k_1^+} - \frac{\vec{k}_{3\perp}^2 + m_3^2}{k_3^+}. \tag{A4}$$

The nonvalence part has the same denominator $D(k-p')$, but $D(k-p)$ is changed to

$$D'(k-p) = p^- - p'^- + \frac{\vec{k}_{3\perp}^2 + m_3^2}{k_3^+} - \frac{\vec{k}_{2\perp}^2 + m_2^2}{k_2^+}. \tag{A5}$$

The energy denominators D_Λ and $D'_{\Lambda'}$ are obtained by the substitutions $m_2 \to \Lambda$ and $m_3 \to \Lambda'$, respectively.

In the case where $m_1 = m_2 = m_3$ and $\Lambda = \Lambda'$ the final formulas are much simplified. The explicit formulas in the main text are valid for the equal-mass case. The general case can be easily constructed from the expressions (A1)–(A5).

In the explicit formulas we use the notation

$$k^\mu = -k_1^\mu, \quad x = \frac{p^+ - k^+}{p^+} \ \text{(valence)},$$

$$x = \frac{k^+ - p^+}{p^+} \ \text{(nonvalence)}, \quad \alpha = \frac{p'^+ - p^+}{p^+}. \tag{A6}$$

APPENDIX B: ANALYTICITY

From the covariant expression for the amplitude one can prove that the form factors are analytic functions of Q^2. This proof is not valid for the LF-time-ordered amplitudes. One can, however, expand the expressions that one obtains for the different parts of the form factor in terms of Q and determine the Q-dependence at small values of Q^2. It turns out that the results depend on the kinematics: it matters in which reference frame one does the calculations.

We use the formulas for the momenta given in Table II and expand the trace and the energy denominators in powers of Q. From this expansion the analyticity properties of the amplitudes follow. We have numerically verified that a blow-up of Figs. 5–8 for small Q^2 illustrates the analyticity properties of the amplitudes discussed in this appendix. The three different reference frames are discussed consecutively.

1. Target-rest frame

We discuss the valence part of the plus-current in detail; the other LF form factors can be treated in a similar way. First we expand the momenta:

$$q^\pm = q\cos\theta + \mathcal{O}(Q^2), \quad \vec{q}_\perp = Q\sin\theta\,\hat{n} + \mathcal{O}(Q^3),$$

$$p'^\pm = M + Q\cos\theta + \mathcal{O}(Q^2), \quad \vec{p}'_\perp = Q\sin\theta\,\hat{n} + \mathcal{O}(Q^3). \tag{B1}$$

The trace consists of a piece that is independent of Q and a piece that consists of two parts, one that is proportional to $Q\vec{k}_{1\perp}\cdot\hat{n}\sin\theta$ and a part proportional to $Q\cos\theta$. The denominator $D(k-p')$ has a similar behavior, but $D(k-p)$ is independent of Q.

Upon integration over $\vec{k}_{1\perp}$ the terms proportional to $\vec{k}_{1\perp}\cdot\hat{n}\sin\theta$ vanish. Consequently, the valence part $F^+_{\rm val}$ has the small-Q behavior

$$F^+_{\rm val} \sim F^{+\,0}_{\rm val} + F^{+\,1}_{\rm val} Q\cos\theta. \tag{B2}$$

The other cases, nonvalence plus-current, valence and nonvalence minus-current, show the same pattern. There are pieces independent of Q, parts with the Q dependence $Q\vec{k}_{1\perp}\cdot\hat{n}\sin\theta$ and ones proportional to $Q\cos\theta$. As the pieces proportional to $\vec{k}_{1\perp}\cdot\hat{n}$ vanish upon integration, all the components of the form factor show a behavior similar to Eq. (B2). So, only for $\theta = \pi/2$ do we find that the LF time-ordered amplitudes calculated in the target-rest frame are analytic in Q^2.

2. Breit frame

In the case of the Breit frame we can follow the same line as in the case of the target-rest frame. The only difference is that now no terms of the form $Q\vec{k}_{1\perp}\cdot\hat{n}\sin\theta$ appear. As those terms give no contribution to first order in Q anyway, this does not alter the result: also in the Breit frame the components of the form factor have the same small-Q behavior as in Eq. (B2).

3. Drell-Yan-West frame

In the Drell-Yan-West frame there is no angle dependence. However, there is a term linear in Q. It is proportional to $Q\hat{n}\cdot\vec{k}_{1\perp}$. Of course, this term also vanishes upon integra-

tion over $\vec{k}_{1\perp}$. Therefore, in the Drell-Yan-West frame we find no term linearly dependent on Q, so the amplitudes are analytic in Q^2.

4. Zero mode

The zero mode is defined as the contribution to the nonvalence amplitude that survives in the limit $q^+ \to 0$. It is easy to see that only the minus-current can have a zero-mode part, because the integral defining $F^+_{\rm nv}$ has an integrand that remains finite when q^+ goes to 0. However, the integrand defining $F^-_{\rm nv}$ diverges when the limit $q^+ \to 0$ is taken. In order to determine the limit, one may expand the integrand in powers of q^+. As q^+ is taken to be zero in the Drell-Yan-West frame, the analysis cannot be done in that frame, but it can most easily be carried out in the Breit frame.

The algebra being straightforward but tedious, we shall not give the details. Rather we quote the final result. If we consider the smeared case, the most divergent part of the integrand for $F^-_{\rm nv}$ has the behavior $1/q^{+2}$. As the integration over k_1^+ ranges from $-p'^+$ to $-p^+$, we can scale the integration variable as in Eq. (A6) and obtain an integral over x from 0 to 1. The Jacobian being q^+, it cancels one factor q^+ in the denominator, so we only need to show that the leading term vanishes to prove that the zero-mode contribution is finite.

Upon carrying out the algebra we find the following result. The leading part is proportional to

$$x^2(\vec{k}^2_{3\perp}+m_3^2)(\vec{k}^2_{3\perp}+\Lambda'^2)-(1-x)^2(\vec{k}^2_{2\perp}+m_2^2)(\vec{k}^2_{2\perp}+\Lambda^2). \tag{B3}$$

This part of the integrand does not vanish, because $\vec{k}_{2\perp}=\vec{p}_\perp-\vec{k}_\perp \neq \vec{k}_{3\perp}=\vec{p}'\perp-\vec{k}_\perp$. However, if we take $\Lambda'=\Lambda$ and $m_2=m_3$, being the mass of the struck quark, and as $\vec{k}_{2\perp}$, $\vec{k}_{3\perp}$, and $\vec{k}_\perp$ differ only by a constant vector, this function vanishes after integration over x from 0 to 1 and $\vec{k}_\perp$ over the whole of $\mathbb{R}_2$. So we see that the coefficient of the contribution proportional to $1/q^+$ vanishes. The remaining part, the piece that survives the limit $q^+ \to 0$, is the zero mode contribution. In the Breit frame as well as the target rest frame it is well-defined and finite.

[1] S.J. Brodsky, H.C. Pauli, and S.S. Pinsky, Phys. Rep. **301**, 299 (1998).

[2] S.J. Brodsky, J.R. Hiller, and G. McCartor, Phys. Rev. D **58**, 025005 (1998); J.R. Hiller, ''Pauli-Villars Regularization in a Discrete Light Cone Model,'' hep-ph/9807245.

[3] C.-R. Ji, Acta Phys. Pol. B **27**, 3377 (1996); H.-M. Choi and C.-R. Ji, Phys. Rev. D **59**, 034001 (1999); **59**, 074015 (1999); Phys. Lett. B **460**, 461 (1999).

[4] B.L.G. Bakker and C.-R. Ji, Phys. Rev. D **62**, 074014 (2000).

[5] S.J. Brodsky and D.S. Hwang, Nucl. Phys. **B543**, 239 (1999); for a recent discussion on effective treatment of nonvalence contribution, see C.-R. Ji and H.-M. Choi, hep-ph/0009281.

[6] S.J. Brodsky, M. Diehl, and D.S. Hwang, hep-ph/0009254.

[7] M. Sawicki and L. Mankiewicz, Phys. Rev. D **37**, 421 (1988); L. Mankiewicz and M. Sawicki, *ibid.* **40**, 3415 (1989).

[8] N.C.J. Schoonderwoerd and B.L.G. Bakker, Phys. Rev. D **57**, 4965 (1998); **58**, 025013 (1998).

[9] S. Głazek and M. Sawicki, Phys. Rev. D **41**, 2563 (1990).

[10] M. Sawicki, Phys. Rev. D **44**, 433 (1991); **46**, 474 (1992).

[11] H.-M. Choi and C.-R. Ji, Phys. Rev. D **58**, 071901 (1998).

[12] S.J. Brodsky and D.S. Hwang, Nucl. Phys. **B543**, 239 (1998).

[13] T. Frederico and G.A. Miller, Phys. Rev. D **45**, 4207 (1992).

[14] L.L. Frankfurt and M.I. Strikman, Nucl. Phys. **B148**, 107 (1979); Phys. Rep. **76**, 215 (1981).

[15] J.P.B.C. de Melo, J.H.O. de Sales, T. Frederico, and P.U. Sauer, Nucl. Phys. **A631**, 574 (1998); J.P.B.C. de Melo, H.W.L. Naus, and T. Frederico, Phys. Rev. C **59**, 2278 (1999).

[16] W. Jaus, Phys. Rev. D **60**, 054026 (1999).

[17] J.C. Ward, Phys. Rev. **78**, 182 (1950); Y. Takahashi, Nuovo Cimento **6**, 371 (1957); for a discussion of moving form factors from the vertices to the propagators that guarantees current conservation, see F. Gross and D.O. Riska, Phys. Rev. C **36**, 1928 (1987).

[18] C.N. Brown *et al.*, Phys. Rev. D **8**, 92 (1973).

[19] P. Brauel *et al.*, Phys. Lett. **69B**, 253 (1977).

[20] H. Ackermann *et al.*, Nucl. Phys. **B137**, 294 (1978).

[21] S.R. Amendolia *et al.*, Nucl. Phys. **B277**, 168 (1986).

[22] J. Volmer, Ph.D. thesis, Vrije Universiteit, Amsterdam, 2000.

[23] S.R. Amendolia *et al.*, Phys. Lett. B **178**, 435 (1986).

[24] C. Caso *et al.*, Eur. Phys. J. C **3**, 1 (1998).

[25] T. Frederico (private communication); see also, J.P.B.C. de Melo, T. Frederico, H.W.L. Naus, and P.U. Sauer, Nucl. Phys. **A660**, 219 (1999).

[26] C.-R. Ji and C. Mitchell, Phys. Rev. D **62**, 085020 (2000).